Validity of the Cauchy-Born rule applied to discrete cellular-scale models of biological tissues

Y. Davit,[1,2,3] J. M. Osborne,[4] H. M. Byrne,[1,4] D. Gavaghan,[4] and J. Pitt-Francis[4]

[1]*Mathematical Institute, University of Oxford, 24-29 St Giles', Oxford, OX1 3LB, United Kingdom*

[2]*Université de Toulouse, INPT, UPS, Institut de Mécanique des Fluides de Toulouse, Allée Camille Soula, F-31400 Toulouse, France*

[3]*CNRS, Institut de Mécanique des Fluides de Toulouse, F-31400 Toulouse, France*

[4]*Department of Computer Science, University of Oxford, Parks Road, Oxford OX1 3QD, United Kingdom*

(Received 11 June 2012; revised manuscript received 13 December 2012; published 30 April 2013)

The development of new models of biological tissues that consider cells in a discrete manner is becoming increasingly popular as an alternative to continuum methods based on partial differential equations, although formal relationships between the discrete and continuum frameworks remain to be established. For crystal mechanics, the discrete-to-continuum bridge is often made by assuming that local atom displacements can be mapped homogeneously from the mesoscale deformation gradient, an assumption known as the Cauchy-Born rule (CBR). Although the CBR does not hold exactly for noncrystalline materials, it may still be used as a first-order approximation for analytic calculations of effective stresses or strain energies. In this work, our goal is to investigate numerically the applicability of the CBR to two-dimensional cellular-scale models by assessing the mechanical behavior of model biological tissues, including crystalline (honeycomb) and noncrystalline reference states. The numerical procedure involves applying an affine deformation to the boundary cells and computing the quasistatic position of internal cells. The position of internal cells is then compared with the prediction of the CBR and an average deviation is calculated in the strain domain. For center-based cell models, we show that the CBR holds exactly when the deformation gradient is relatively small and the reference stress-free configuration is defined by a honeycomb lattice. We show further that the CBR may be used approximately when the reference state is perturbed from the honeycomb configuration. By contrast, for vertex-based cell models, a similar analysis reveals that the CBR does not provide a good representation of the tissue mechanics, even when the reference configuration is defined by a honeycomb lattice. The paper concludes with a discussion of the implications of these results for concurrent discrete and continuous modeling, adaptation of atom-to-continuum techniques to biological tissues, and model classification.

DOI: 10.1103/PhysRevE.87.042724 PACS number(s): 87.18.Fx, 87.19.rd

I. INTRODUCTION

Biological tissues are multiscale entities. Processes involved in their functioning occur over a broad spectrum of temporal and spatial scales. In tumor development, for example, genetic and epigenetic modifications disrupt cell homeostasis at the molecular level (DNA damage and mutations), leading to anomalous behaviors at the cellular-level (apoptosis and abnormal proliferation) and tissue-level (morphogenesis and angiogenesis) growth. Within communities of micro-organisms attached to solid or liquid interfaces, micrometer-size microbes can form intricate millimeter-size structures (or smaller) interspersed with submillimeter fluid channels, termed biofilms. Furthermore, time scales may vary from milliseconds, for flow or signal transduction, to years, for significant tissue growth. Although there have been significant advances in our computational capabilities, simulating at the molecular scale over a period of several years is currently infeasible. In order to address these issues, a variety of theoretical approaches have been developed to model biological tissues (see discussions in [1,2]), leading to the emergence of two paradigms: discrete (cellular) and continuum (tissular) representations. In the remainder of this work, we will focus on passive (i.e., without growth) tissue mechanics as described by these two paradigms.

Within a cellular representation, all cells are modeled as discrete entities that can proliferate, migrate, die, and interact with neighboring cells. This can be achieved in several different ways, including on-lattice descriptions for which cells and processes are represented on a fixed regular grid. Examples of on-lattice representations are cellular automata (see [3]) and cellular Potts models (also known as Graner-Glazier models; see [4]). By contrast, off-lattice models represent each cell by a set of points in space, independently of any grid. Examples of off-lattice models include center-based models where cells are represented by a single point (e.g., sphere-based models in [5] or tessellation-based models in [6]) and vertex-based models (see [7]) where cells are represented by their vertices. Further models, known as subcellular element models, where cells are comprised of a collection of points, are an extension to traditional center-based models (see [8]). These biological models share some similarities with discrete element methods (DEMs) (see, for example, [9]) used in material and soft matter sciences to describe, among other substances, granular matter, powders, foams, or fracturing solids. However, unlike material and soft matter sciences, constitutive relations for biological tissue mechanics are not well understood. An important consequence is that DEMs are elaborated on the basis of strong physical grounds, whereas cellular-scale biological models are treated in a simple conceptual manner (e.g., center-based spring forces). In this paper, we will focus on simple cellular-scale models and will not extend our results to more complicated DEMs.

With the continuum representation, the tissue is modeled via a system of partial differential equations (PDEs). The PDEs can also be discretized to allow for numerical solution but, in contrast with cellular-scale models, a typical mesh size will be much coarser than the characteristic length of

a cell. Tissues are therefore described in an averaged sense, with properties evaluated between the cellular and tissular scales. Within this framework, tissue mechanics typically rely on linear or nonlinear elastic or viscoelastic theories and cellular growth is introduced through constitutive evolution laws for macroscale parameters. One such method is based on a multiplicative decomposition of the deformation gradient $\mathsf{F} = \mathsf{F}_p \cdot \mathsf{F}_a$, where F_a represents the imposed (active) growth and F_p is the (passive) mechanical response. Another approach relies upon an additive decomposition: the Piola-Kirchhoff stress tensor (see [10] for a detailed discussion of these models).

The two classes of models introduced above have their respective strengths and weaknesses. Cellular-scale descriptions can incorporate a substantial amount of information that may be particularly relevant to medical and biological applications. In tumor development, for instance, initial mutations occur within individual cells, a phenomenon that can only be adequately understood using cellular-scale models. Obviously, the disadvantage of such resolution is the computational expense, which exceeds current capabilities when dealing with large numbers of cells, for example, when considering entire organs or even organisms (e.g., $\approx 10^{14}$ cells in the human body). Further, these models are often based on mathematical abstractions that can be difficult to relate to biophysically measurable properties associated with the problem of interest. Continuum-based approaches, in contrast, are less computationally intensive and provide a more intuitive framework in which parameters and operators can be adjusted to fit experimental observations. However, they describe only an average behavior of the tissue and have domains of validity that can be difficult to determine.

Although continuum and cellular-scale approaches have traditionally been used separately, there is evidence that they could be used in a complementary manner. Recent works have proposed such multiscale methods that aim to overcome issues with computational limitations without sacrificing precision. Hybrid concurrent discrete-continuous models, for instance, may be used for such purposes. Hybrid frameworks rely on the idea that, in many cases, a cellular-scale description is needed only in a limited region of the tissue where processes vary over short spatial or temporal scales. In the rest of the tissue, where characteristic times and lengths are significantly larger, continuum descriptions may be used. Kim and co-workers [11,12] applied this idea to tumor spheroids, using a continuum approach to model the necrotic and quiescent zones and a discrete cellular-scale model within the relatively small and active peripheral region. From a practical point of view, such models are extremely appealing because they resolve many of the issues found when each approach is used individually: the computational cost of pure cellular-scale models and the failure of continuum models to capture phenomena occurring on short scales. From a more fundamental perspective, however, there are a number of issues that require attention before this approach can be more widely used to develop models of biological tissues. The following are typical unresolved questions. What boundary conditions should be imposed on the interface between discrete and continuum regions? Where should the interface be positioned? How should it evolve over time?

Interestingly, similar problems have emerged in atom-to-continuum (ATC) modeling where various multiscale strategies have been developed to deal with large deformations and dislocations in crystalline systems. Such multiscale methods include quasicontinuum (QC) [13], bridging scale [14], hybrid discrete-continuum with blending [15], or nonlocal [16] techniques. Blending techniques, for example, are used to treat boundaries in hybrid discrete-continuum formulations. Continuity conditions are imposed at the interface between the two distinct regions by defining an overlapping volume that is used to blend model variables, e.g., energy functionals, forces, stresses, or displacements (see [17]). Another category of models, termed QC methods (see [18] for a thorough review of QC methods), aims to approximately solve the atomic-scale problem. The technique uses adaptive meshing and interpolation procedures inherited from finite element methods, in conjunction with physical approximations that allow for the reduction of the number of degrees of freedom of the problem [localization, Cauchy-Born rule (CBR), strain and stress criteria, and representative atoms]. Peridynamic models are spatial nonlocal formulations that describe material mechanics by using an integral formulation of momentum transport, an approach that avoids issues associated with cumbersome boundary conditions of concurrent models. For all of these models, however, a means of bridging discrete and continuum scales is needed in order to develop clear relationships between both paradigms. With hybrid modeling, for instance, the model used in the continuum region should correspond, in some sense, to the continuum limit of the discrete model and boundaries should be treated accordingly.

For cellular-scale models, this discrete-to-continuum connection has been most widely studied in one spatial dimension and is not yet available in higher-dimensional configurations. For example, Murray *et al.* [19] derived a continuum expression corresponding to a one-dimensional (1D) chain of overdamped cells. In this approach, the limit of discrete sums is considered to obtain differential operators that can be combined into a single nonlinear diffusion equation for cellular density. Bodnar and Velasquez [20] studied the mathematical behavior of an integro-differential (nonlocal) equation for the cellular density that can be interpreted as the continuum limit of a 1D tissue model of overdamped particle interacting via conservative forces. Fozard *et al.* [21] used asymptotics to derive Darcy-like equations for momentum transport at the continuum scale. These approaches pave the way for future developments and provide insight into the large-scale dynamics of cellular-scale models. However, their extension to higher-dimensional systems is not systematic. To illustrate the complexity inherent to higher-dimensional systems, let us consider an off-lattice model with spring interactions between closest neighbors and the connectivity determined via a Voronoi tessellation. Compared to a finite volume discretization of an isotropic elastic material, the cell-based model ignores tangential (bending) forces. Therefore, even this simple network of springs cannot be assimilated to an elastic material and the continuum limit, if it exists, will depend on many parameters, including the level of disorder in the network, the average connectivity (see [22]), and the distribution of prestress. Such 2D or 3D extensions are important because they provide a solid basis for (i) relating the effective

tissue-scale parameters to cellular-scale properties, (ii) understanding the approximations associated with continuum models and establishing when continuum approaches are appropriate, (iii) developing appropriate boundary conditions for hybrid concurrent models or adapating other ATC strategies to the biological context, and (iv) creating classification methods for cellular-scale models via their continuum limit.

For crystal mechanics, this bridge can be obtained using the CBR. The CBR is an assumption that can be used to pass information through scales by linearly relating the local microscale displacement field to the mesoscale deformation gradient. In this study, our goal is to analyze numerically the validity of the CBR for cellular-scale models of biological tissues with honeycomb and disordered reference states. We will focus solely on passive tissue mechanics, i.e., we will not consider cellular growth. To this end, we will use an approach similar to that of Aghaei *et al.* [23] and Friesecke and Theil [24]. We will consider a representative region of the tissue, impose an affine deformation on boundary nodes, and calculate an average deviation from the CBR in the central region.

The remainder of this work is organized as follows. In Sec. II, we discuss in more detail the CBR and ideas underlying its application to cellular-scale models of biological tissues. In Sec. III, we present the modeling framework and the implementation of these models. In Sec. IV, we present results and their interpretation. Finally, in Sec. V, we discuss the implications of these results for discrete-to-continuum approaches, hybrid discrete-continuous modeling, and model classifications.

II. CAUCHY-BORN RULE

A. Definitions

The CBR was used by Cauchy [25] and Born [26] to derive expressions for the elastic modulus of a crystalline solid in terms of atomic-scale parameters. The rule is illustrated in Fig. 1 and arises from the following considerations (see detailed discussion in [27]). First, consider a homogeneous crystalline material, characterized by the macroscopic length scale L, and a unit cell for the crystal structure, characterized by the microscopic length scale ℓ. Suppose that a macroscopic stress or strain with a characteristic time τ_M initiates a deformation of this material and that relaxation at the microscopic scale is characterized by the time τ_μ. Now, impose the separation of length scales $L \gg \ell$ so that each unit cell can be treated as a macroscopic point and the deformation gradient F can be considered to be constant over each unit cell. Finally, assume that there is a separation of time scales $\tau_M \gg \tau_\mu$ so that the relaxation processes within each unit cell can be considered quasisteady. The CBR states that all atoms within each unit cell will be displaced homogeneously. In other words, if $\mathbf{r}_i$ ($\mathbf{r}_j$) is the quasisteady position of atom i (j) in the stressed state and $\mathbf{R}_i$ ($\mathbf{R}_j$) is the position of atom i (j) in the reference configuration, then

$$\mathbf{r}_{ij} \equiv \mathbf{r}_i - \mathbf{r}_j = \mathsf{F} \cdot (\mathbf{R}_i - \mathbf{R}_j) = \mathsf{F} \cdot \mathbf{R}_{ij}. \tag{1}$$

In conjunction with this relationship, a variety of methods can be used to derive the macroscale continuum equations. For example, methods based on discrete expressions of the Cauchy stress tensor [28] or strain density energies may be used.

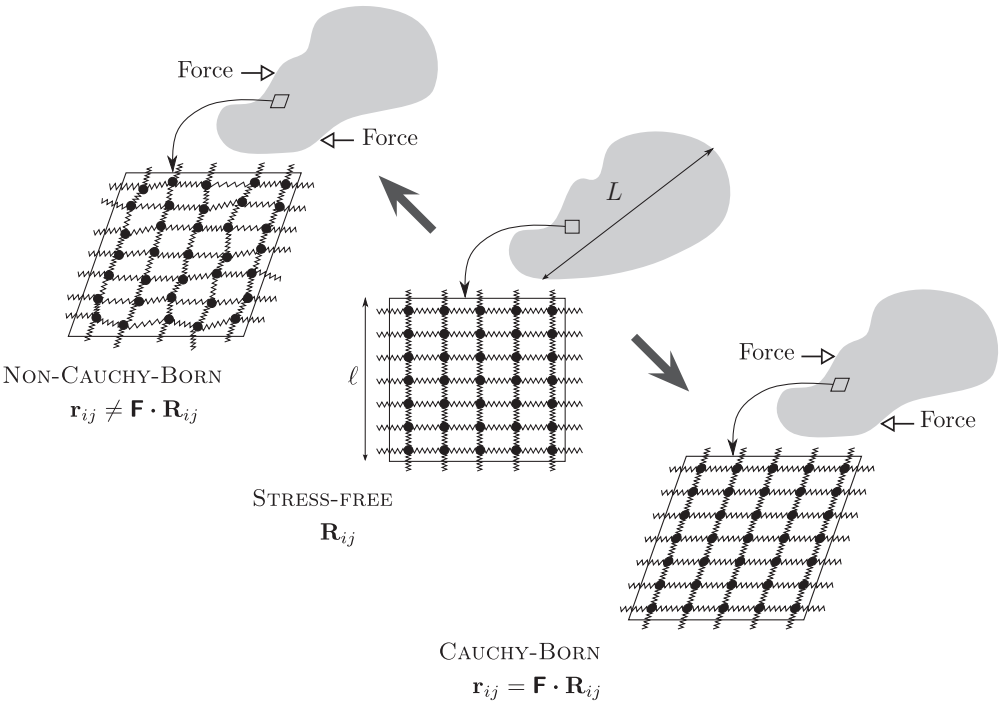

FIG. 1. Schematic representation of the CBR. The central picture shows the node positions in the reference (lattice) configuration. In the two other figures, forces applied at a macroscopic level induce deformation of the material. The bottom right configuration corresponds to displacements that satisfy the CBR, while the top left configuration describes displacements that do not, i.e., nodes are rearranging on an atomic length scale.

B. Noncrystalline reference state

The CBR does not generally apply to noncrystalline materials because deformations occur inhomogeneously, i.e., stresses generate reorganization and relaxation of the (quenched) reference state on small length scales. However, it can be used to approximate amorphous solid continuum mechanics (see [29]), even though the calculation of effective properties may require the expression of the residual stresses in the reference state. In this work, the rationale for studying the validity of the CBR when applied to cellular-scale models of biological tissues is fourfold.

(i) As discussed in [29], the validity of the CBR at the microscale translates the intuitive notion of solid behavior at the macroscale: Displacements about a stable equilibrium are locally homogeneous and do not generate node permutations, as is the case for fluids. In this sense, studying the validity of the CBR is similar to studying elastic continuum properties of biological tissues.

(ii) The affine displacement field may be considered as a reference state for tissue mechanics and comparisons with this reference may provide useful information. For instance, Goldenberg *et al.* [30] showed that, for a 2D Lennard-Jones glass, the nonaffine field may be characterized by a notion of local defects and a scalar noise.

(iii) We will focus on structured reference states for which the CBR may be used as a first-order approximation to calculate homogenized continuum stresses and energies. Example tissues that exhibit spatially structured patterns include plants, wood, leaves, bones, ocular tissues, sponges, and epithelia (see, e.g., [31]). Two of the most common patterns are foamlike and honeycomb structures. Furthermore, the honeycomb reference state has often been used for modeling purposes. Therefore, honeycomb results can be used to study model mechanical behavior in the continuum limit, for example to provide a means of comparison between cellular-scale models.

(iv) Tissue mechanics and morphogenesis are governed by a complex dynamical interplay between, e.g., extracellular substances, fluids, cell membranes, cell cytoskeleta, and intercellular protein junctions (see [32]). In these systems, large networks of biopolymers generate intercellular interactions that strengthen the elastic behavior of the tissue as a whole. In particular, fiber networks are known to behave in a self-similar (affine) manner in some regions of parameter space (see [33,34]).

III. MODELING FRAMEWORK

A. Cellular-scale models and CHASTE

The computations presented in this paper were performed using CHASTE (cancer, heart, and soft-tissue environment), an open-source modeling framework developed in C++ by the Department of Computer Science at the University of Oxford. CHASTE includes a set of libraries and test suites for cellular-scale models of biological tissues with on-lattice and off-lattice descriptions. CHASTE also handles cellular growth and provides various generic solvers for differential equations and boundary value problems that can be used for coupling cellular-scale models with systems of ordinary differential equations and PDEs. Further information about the code can be found in [35,36].

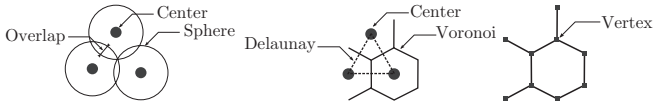

(a) Center-based Sphere-based (b) Center-based Tessellation-based (c) Vertex-based Fixed-connectivity

FIG. 2. Schematics of the different modeling frameworks.

In this work, we will use the 2D off-lattice cellular-scale models of CHASTE; in particular we use two classes of models that we characterize as follows. Center-based models (see [37]) simulate cell movement by concentrating mass at its center, hence reducing computations to tracking a finite number of nodes (cell centers). Vertex-based models (see [7,39]) view cells as polygons that can be characterized by the positions of their vertices. When considering center-based models, we will distinguish between sphere- and tessellation-based models, which differ in the way in which connectivity is determined, i.e., how neighbors are defined. For sphere-based models, connectivity is resolved via a radius of interaction [see Fig. 2(a)]. For tessellation-based models, connectivity is resolved using a Voronoi tessellation and the corresponding Delaunay triangulation [see Fig. 2(b)]. For vertex-based models, connectivity is defined by a network of connected polygons [see Fig. 2(c)]. When considering vertex-based models we will only consider cases for which connectivity is determined by the initial configuration.

For each model, we assume that cell movement is overdamped, so that applying Newton's law of motion to each node i supplies

$$\eta_i \frac{d\mathbf{r}_i}{dt} = \mathbf{f}_i, \tag{2}$$

where η_i is a damping coefficient or viscous drag that we set equal to 1.0 nN h μm^{-1} for each node, $\mathbf{r}_i$ is the position of node i (μm), t is the time variable in hours, and $\mathbf{f}_i$ is the force on node i in nanonewtons. We discretize Eq. (2) using a forward Euler method so that the position of node i at time $t + \Delta t$ is determined from its position at time t via

$$\mathbf{r}_i^{t+\Delta t} = \mathbf{r}_i^t + \frac{\Delta t}{\eta}\mathbf{f}_i. \tag{3}$$

Stability of the explicit discretization method requires that the time step is carefully chosen. Here we used $\Delta t = \frac{1}{120}$ h $=$ 30 s for center-based models and $\Delta t = 1.8$ s for vertex-based models, which were found to exhibit a greater time step sensitivity.

To complete our characterization of these cellular-scale models, we must define constitutive laws for the forces $\mathbf{f}_i$. For center-based models, we express these forces in terms of the nondimensionalized overlap parameter

$$\delta = \frac{1}{\ell}(\|\mathbf{r}_{ij}\| - \ell_{ij}), \tag{4}$$

where $\ell_{ij} > 0$ is the rest length of the spring that connects nodes i and j, ℓ is a characteristic length scale (which we set equal to 10 μm), and δ can be interpreted as a measure of the deviation from the rest length with a sign that determines the nature (attractive or repulsive) of the force. Unless stated otherwise, we assume that rest lengths are identical for all cells

TABLE I. Summary of the four models used in this paper. Each model is completely defined by a type (cellular or vertex based), a notion of connectivity (sphere based, tessellation based, or initially fixed), and a force (S, QS, NL, or NH).

Model	Type	Connectivity	Force
1	center based	tessellation based	spring $\mathbf{f}_i^S$
2	center based	sphere based	quasispring $\mathbf{f}_i^{QS}$
3	center based	sphere based	nonlinear $\mathbf{f}_i^{NL}$
4	vertex based	fixed	Nagai-Honda $\mathbf{f}_i^{NH}$

within the population and equal to ℓ. This may be written as $\ell_{ij} = \ell$ for any pair i, j. For center-based models, we will use a cutoff length $\ell_c = 1.1 \times \ell$, which enforces a finite distance of interaction between cells. In the remainder of this paper, we consider spring (S), quasispring (QS), and nonlinear (NL) forces for center-based models and a Nagai-Honda (NH) force for the vertex-based model. Details of all forces are given in the Appendix and models are summarized in Table I. For clarity, from here on, we will refer to each model by the number assigned to it in this table.

B. CBR tests

For ATC problems, the validity of the CBR has been studied in various systems. For example, Friesecke and Theil [24] studied analytically the behavior of a network of atoms, initially positioned on a 2D square lattice and interacting via harmonic springs. By prescribing an affine deformation on boundary nodes of a unit cell and studying the response of central nodes, they showed that particle locations predicted by the CBR are a minimizer of the net energy only in a limited region of parameter space. In particular, the validity of the CBR is restricted to relatively small deformation gradients. Aghaei *et al.* [23] studied the validity of the CBR numerically on a lattice of atoms interacting via the Sutton-Chen many-body potential. They also imposed a deformation on boundary atoms and observed the response of central atoms. By examining deviations from the CBR in the strain and stress domains, they could determine domains of validity. In this paper, we will apply a similar strategy to the cellular-scale models discussed above. In Fig. 3 we illustrate how we distinguish between boundary and central nodes for a tessellation-based model.

Herein, positions are resolved within a Cartesian coordinate system that has its origin at the center of mass of the cell population. The x and y axes are oriented along natural horizontal and vertical directions (see Fig 3). Boundary nodes are displaced from positions $\mathbf{R}_i$ in the reference state to $\mathbf{r}_i$ by introducing a mesoscale deformation gradient F so that

$$\mathbf{r}_i = \mathsf{F} \cdot \mathbf{R}_i. \tag{5}$$

Further, tension and compression and shear deformations are applied by using the following two tensors $\mathsf{F}^{\mathrm{T,C}}$ and F^{S}:

$$\mathsf{F}^{\mathrm{T,C}} \equiv \begin{bmatrix} 1 & 0 \\ 0 & \alpha_{\mathrm{T,C}} \end{bmatrix} \tag{6}$$

and

$$\mathsf{F}^{\mathrm{S}} \equiv \begin{bmatrix} 1 & \alpha_{\mathrm{S}} \\ 0 & 1 \end{bmatrix}. \tag{7}$$

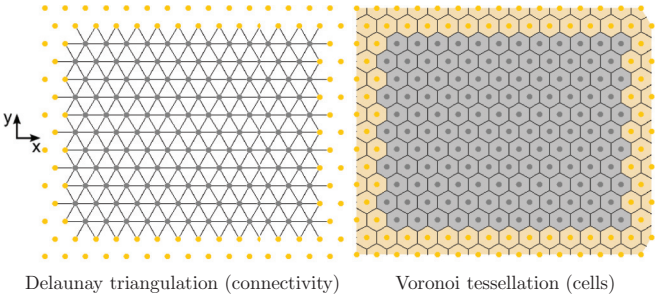

FIG. 3. (Color online) Example population of center-based tessellation-based cells. The Delaunay triangulation is plotted on the left-hand side and the corresponding Voronoi tessellation is plotted on the right-hand side. Boundary cells to which displacements are applied are colored in yellow. Central cells that are used to study deviations from the CBR are colored in gray. We remark that there is a top-bottom reflection symmetry but no left-right symmetry.

Here the deformation constant α sets the amplitude of the deformation. We remark that with these notations, the reference configuration is given by $\alpha_{\mathrm{T,C}} = 1$ for tension and compression and $\alpha_{\mathrm{S}} = 0$ for shear.

For a given target value of α, boundary nodes were displaced by small increments $\Delta\alpha = 2 \times 10^{-3}$ for center-based models and $\Delta\alpha = 1 \times 10^{-3}$ for vertex-based models. For center-based models, the system was assumed to be at equilibrium when either the average velocity over all nodes reached the critical value $10^{-7}\ \mu\mathrm{m}\ \Delta t^{-1}$ or the total time for relaxation of this α increment reached 10 h. For vertex-based models, the system was assumed to be at equilibrium when either the average velocity over all nodes reached the critical value $10^{-10}\ \mu\mathrm{m}\ \Delta t^{-1}$ (vertex-based models exhibited a greater sensitivity to the α increment) or the total time for relaxation of this α increment reached 10 h. Although results are not presented here, tests for convergence were performed by repeating the simulations using fractions of these time steps and α increments. In some cases, presented below, we also imposed small perturbations, i.e., random motion of the cells, to further explore the stability of our results. This method was implemented by selecting, for each time step, a random direction and enforcing a small jump of the node in this direction with a velocity of $10^{-1}\ \mu\mathrm{m\,h}^{-1}$, i.e., an amplitude of $\approx 8.3 \times 10^{-4}\ \mu$m for a time step $\Delta t = \frac{1}{120}$ h. For simplicity, we refer to such random displacements as Brownian, although they are not meant to describe Brownian motion but to address the sensitivity of our results to small perturbations. For simulations without random displacements, we will use the term non-Brownian.

The validity of the CBR was evaluated by comparing, in the strain domain, the computed positions of the central nodes with the predictions of the CBR [see Eq. (1)]. Deviation was measured via the expression

$$(\text{deviation}) \equiv \frac{1}{\ell N} \sum_{i=1}^{N} \left\| \mathbf{r}_i - \mathbf{r}_i^{\mathrm{CBR}} \right\| = \frac{1}{\ell N} \sum_{i=1}^{N} \left\| \mathbf{r}_i - \mathsf{F} \cdot \mathbf{R}_i \right\|, \tag{8}$$

where N is the total number of nodes, $\mathbf{r}_i$ is the computed position of node i, and $\mathbf{r}_i^{\mathrm{CBR}}$ is the position of node i predicted

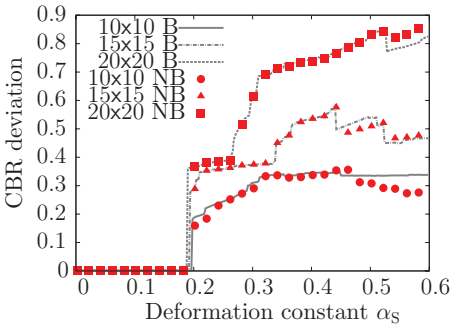

(a) Shear

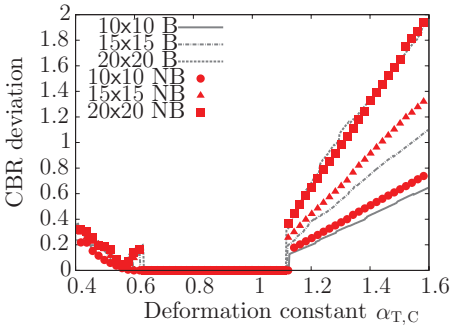

(b) Tension and compression

FIG. 4. (Color online) Series of plots showing how model 1 (center based and tessellation based) deviates from the CBR as the deformation parameter α varies for (a) shear and (b) tension and compression deformations. For each plot, three sizes of tissues are presented (10×10, 15×15, and 20×20 cells) for Brownian (B) and non-Brownian (NB) cases. Results were obtained by computing Eq. (8) in the central region for displacements prescribed on the boundary nodes using Eqs. (5)–(7). These plots show that (i) the CBR is valid only in the limit of small deformations; (ii) the domain of validity is independent of the size of the tissue for the non-Brownian case; (iii) for the Brownian case, the domain of validity of the CBR slightly decreases with an increase in the size of the tissue; and (iv) domains of validity are relatively robust to perturbations.

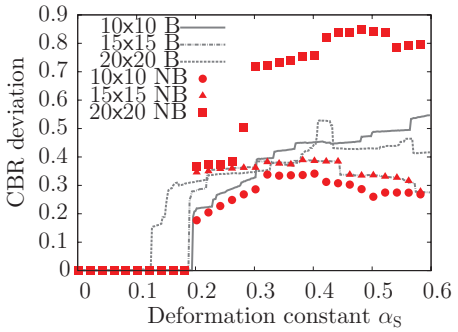

(a) Shear

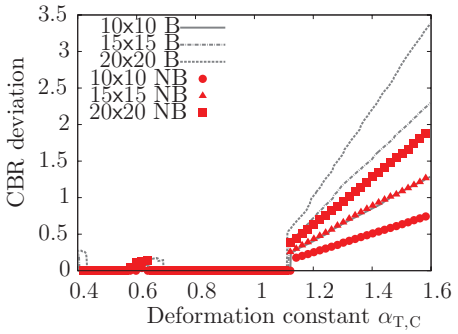

(b) Tension and compression

FIG. 5. (Color online) Series of plots showing how model 2 (center based and sphere based) deviates from the CBR as the deformation parameter α varies for (a) shear and (b) tension and compression deformations. For each plot, three sizes of tissues are presented (10×10, 15×15, and 20×20 cells) for Brownian and non-Brownian cases. Results were obtained by computing Eq. (8) in the central region for displacements prescribed on the boundary nodes using Eqs. (5)–(7). These plots show that (i) the CBR is valid only in the limit of small deformations; (ii) the domain of validity is independent of the size of the tissue for the non-Brownian case; (iii) for the Brownian case, the domain of validity of the CBR slightly decreases with an increase in the size of the tissue; and (iv) domains of validity are relatively robust to perturbations.

by the CBR. We remark that different measures are available, in particular in the stress domain. We limit our analysis to the strain domain because it yields a natural estimate of this deviation and does not rely on a cumbersome definition of the discrete stress tensor.

IV. RESULTS

A. Center-based models: Models 1, 2, and 3

In this section, we focus on center-based models 1, 2, and 3 (see Table I) and study the validity of the CBR for three sizes of tissue 10×10, 15×15, and 20×20 cells.

1. Honeycomb

Here, nodes are arranged on a honeycomb lattice, similar to the one shown in Fig. 3 for a tessellation-based model. This situation corresponds to a stress-free configuration with constant rest lengths imposed between connected pairs of nodes throughout the population.

For model 1, the deviation Eq. (8) is plotted as a function of the deformation parameter α for shear in Fig. 4(a) and for compression and tension in Fig. 4(b). Results are presented for different sizes of tissue and with (B) or without random motion (NB). Equivalent plots for model 2 are presented in Figs. 5(a) and 5(b). These results show that both models exhibit qualitatively similar behaviors. We remark that the domain of validity of the CBR is limited to the small deformations regime, i.e., relatively small values of α. This result is compatible with theoretical analyses obtained for simpler harmonic spring networks (see [24]). We note also that (i) for the Brownian case, the domain of validity of the CBR slightly decreases with an increase in the size of the tissue, which is primarily due to the appearance of higher deformation modes and was also observed in [23]; (ii) for the non-Brownian case, the size of the tissue does not affect the domain of validity of the CBR, which results from the homogeneity of the geometry; (iii) the amplitude of the average deviation increases with an increase in the size of the tissue in the large deformation regime, when the CBR fails to describe node locations accurately; and

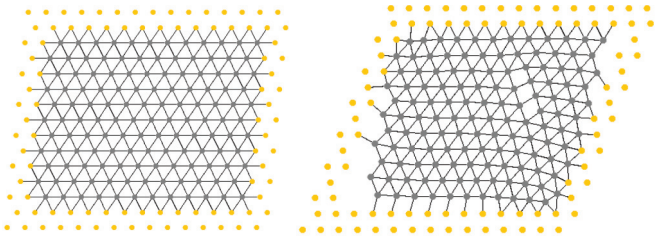

(a) Shear $\alpha_S = 0.1$ (b) Shear $\alpha_S = 0.4$

FIG. 6. (Color online) Sequence of events corresponding to a shear deformation applied to a non-Brownian cell population (15 × 15 cells) described using model 1 for (a) $\alpha_S = 0.1$ and (b) $\alpha_S = 0.4$. The CBR is valid in the limit of small deformations and fails if α_S exceeds a critical value (here $\alpha_S \sim 0.2$) at which strains in the narrowed corners become large enough.

(iv) bifurcation of results for Brownian tension experiments occurs primarily in the large deformation regime where the CBR fails. This shows stability to small perturbations in domains of CBR validity for this configuration.

To understand further why the CBR fails in the large deformation limit, node positions for the tests described above are illustrated for shear experiments, in Fig. 6 for model 1 and in Fig. 7 for model 2. In both cases, the tissue deforms homogeneously [Figs. 6(a) and 7(a)] until α reaches a critical value at which the strain induced in the narrowed portion of the tissue becomes sufficiently large to create local dislocations [Figs. 6(b) and 7(b)]. The dislocations induce a rearrangement of the nodes and their connectivity, leading to failure of the CBR. As α is increased through this critical value, the deviation from the CBR grows approximately linearly, as the size of the dislocations grows.

The spatial organization of nodes for the tension and compression experiments for model 1 are presented in Fig. 8. In the compressive regime, we observe that when α_S reaches a critical value, cellular connectivity is altered. Cells positioned in a given layer are influenced by cells up to two layers away because of how the model is set up, i.e., if cells from distant layers get close enough a new spring connection will link them. This is visible in the Delaunay triangulation representation Fig. 8(a), where the initial connectivity is altered and

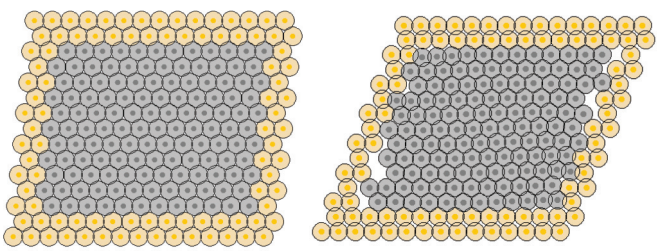

(a) Shear $\alpha_S = 0.1$ (b) Shear $\alpha_S = 0.4$

FIG. 7. (Color online) Sequence of events corresponding to a shear deformation applied to a non-Brownian cell population (15 × 15 cells) modeled using model 2 with (a) $\alpha_S = 0.1$ and (b) $\alpha_S = 0.4$. The CBR is valid in the limit of small deformations and fails if α_S exceeds a critical value (here $\alpha_S \sim 0.2$) at which strains in the narrowed corners regions become large enough.

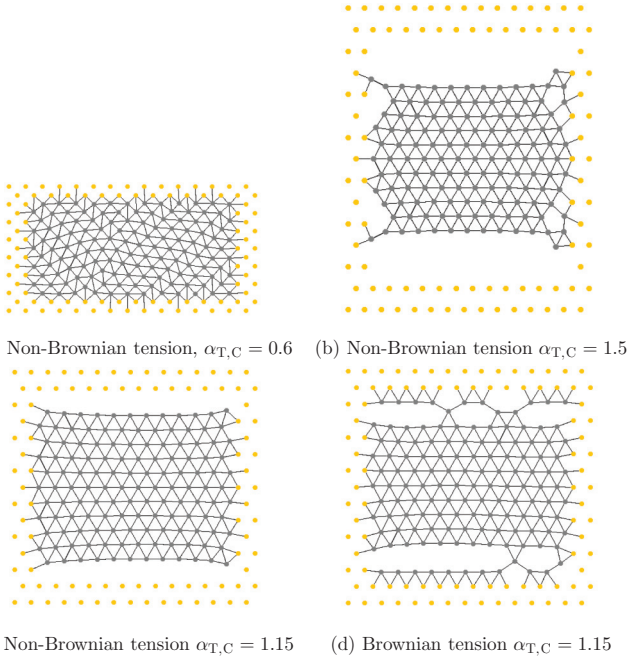

(a) Non-Brownian tension, $\alpha_{T,C} = 0.6$ (b) Non-Brownian tension $\alpha_{T,C} = 1.5$

(c) Non-Brownian tension $\alpha_{T,C} = 1.15$ (d) Brownian tension $\alpha_{T,C} = 1.15$

FIG. 8. (Color online) Sequence of events corresponding to compression and tension deformations of Brownian and non-Brownian cell populations (15 × 15 cells) described by model 1 with (a) $\alpha_{T,C} = 0.6$ non-Brownian tension, (b) $\alpha_{T,C} = 1.5$ non-Brownian tension, (c) $\alpha_{T,C} = 1.15$ non-Brownian tension, and (d) $\alpha_{T,C} = 1.15$ Brownian tension. The CBR is valid in the limit of small deformations and fails if $\alpha_{T,C}$ exceeds a critical value at which either cell connectivities are modified or dislocations appear.

some (gray) central nodes interact with the second layer of (yellow) boundary nodes. This reorganization destabilizes the homogeneous configuration, causing the CBR to fail. Under tension, the tissue is stretched homogeneously until the vertical connections between internal and boundary cells reach their cutoff length. Incrementing α further causes the distance between the nodes to exceed the cutoff length, generating dislocations [see Fig. 8(b)]. Thereafter, the deviation from the CBR increases approximately linearly with $\alpha_{T,C}$ as the size of the dislocations grows. We remark that the slope of this linear dependence is weakly dependent on the Brownian perturbation. Indeed, small perturbations dominate tissue behavior at the onset of plasticity when even the slightest changes in node positions can lead to the appearance of dislocations and the loss of tissue symmetry [compare Figs. 8(c) and 8(d)].

Figure 9 reveals that a similar situation occurs for model 2. Under tension, the qualitative behavior replicates that seen for model 1. Figure 9(a) shows the position of the nodes after the appearance of the dislocation, while Fig. 9(b) shows how symmetry breaking is induced by Brownian perturbations. The main difference between models 1 and 2 is assessed within their response to compressive loading. Figure 9(d) shows that the CBR fails for model 2 when $\alpha_{T,C} \approx 0.6$, but that further compression takes the average deviation back to zero [see Fig. 9(c)]. This behavior is due to the implementation of the sphere-based models. In our model, the radius of interaction of each cell is fixed initially and does not depend on loading. Therefore, under sufficient compression, interactions

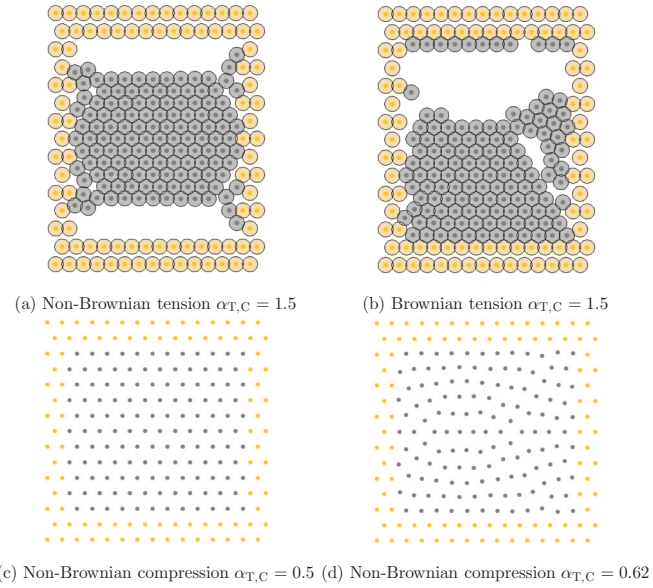

(a) Non-Brownian tension $\alpha_{T,C} = 1.5$ (b) Brownian tension $\alpha_{T,C} = 1.5$

(c) Non-Brownian compression $\alpha_{T,C} = 0.5$ (d) Non-Brownian compression $\alpha_{T,C} = 0.62$

FIG. 9. (Color online) Sequence of events corresponding to compression and tension deformations applied to Brownian and non-Brownian cell populations (15×15 cells) described via model 2 with (a) $\alpha_{T,C} = 1.5$ non-Brownian tension, (b) $\alpha_{T,C} = 1.5$ Brownian tension, (c) $\alpha_{T,C} = 0.5$ non-Brownian compression (rescaled for visualization), and (d) $\alpha_{T,C} = 0.62$ non-Brownian compression (rescaled for visualization). The CBR is valid in the limit of small deformations and fails if α exceeds a critical value for which either cell connectivities are modified or dislocations appear. (c) and (d) illustrate the peculiar behavior of sphere-based models with constant radii of influence for which the CBR fails for a finite range of values of α before becoming valid again in the limit of large compression.

are not limited to closest neighbors. In this limit, internal nodes will also interact with both layers of boundary nodes and these additional forces will force homogeneity of cell displacements. Although this model is physically unrealistic, it results from simplifications made in many sphere-based models and is representative of their mechanical behavior under large compressive loading.

To explore further this effect of radius, we studied the response of the model for a smaller value of the cutoff length, which is equal to the rest length. Results are plotted in Fig. 10(a) for non-Brownian tests. We remark that, in this case, the CBR is not valid under tension because we have eliminated attractive forces. In addition, it seems that the behavior described above persists only for the smallest tissues (10×10 and 15×15 cells) and is not observed for the larger ones (20×20 cells) for which boundary effects are less important. This suggests that the dominant effect is indeed due to the nonlocal interactions between internal and boundary nodes. This was further confirmed by studying the effect of the force using a different nonlinear force, model 3, with a cutoff length of 1.1. The results presented in Fig. 10(b) are similar to those obtained with the quasispring force under compressive loading and show that the QS and NL forces, although different, exhibit equivalent behavior on the tissue scale. This corroborates the conjecture that the anomalous behavior is induced by nonlocal interactions with boundary nodes and not by the nonlinear nature of the forces.

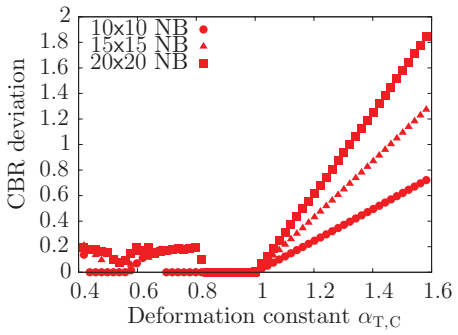

(a) Model 2, $\ell_c = \ell$

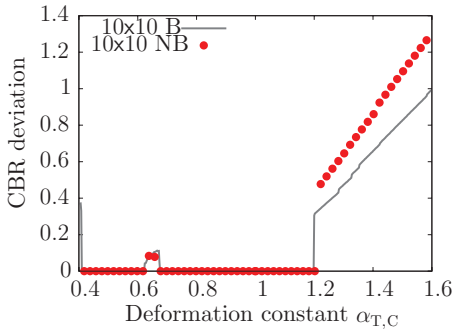

(b) Model 3

FIG. 10. (Color online) Series of plots showing how (a) model 2 (center based and sphere based) with $\ell_c = \ell = 10\ \mu$m and (b) model 3 deviate from the CBR as the deformation parameter α varies under tension and compression. (a) Three sizes of tissues are presented (10×10, 15×15, and 20×20 cells) for the non-Brownian case. (b) One size of tissue is presented (10×10 cells) for the Brownian and non-Brownian cases. Results were obtained by computing Eq. (8) in the central region for displacements prescribed on the boundary nodes using Eqs. (5)–(7). These plots show that (i) the peculiar behavior of sphere-based models with constant radius of interaction disappears as either the size of the tissue is increased or the radius of interaction is reduced; (ii) for $\ell_c = \ell$, the CBR is invalid under tension; and (iii) using the NL or QS forces for a sphere-based population does not modify the qualitative deviation from the CBR.

2. *Disordered reference structures*

In the previous section, the honeycomb (stress-free) reference configuration was obtained by using constant values of the rest lengths for intercellular forces. To investigate the effect of disorder in the reference state on the validity of the CBR, we consider a case for which the rest lengths are chosen from a normal distribution. We set the mean of this Gaussian distribution to be $\ell = 10\ \mu$m and investigate how the standard deviation influences the average deviation from the CBR. The simulated tissue is generated by placing cells on a honeycomb lattice and allowing it to relax to a stable equilibrium before applying any deformation. For each value of the standard deviation ($\frac{\sigma}{\ell} = 0.03$, 0.06, and 0.09), three replicate experiments were performed to account for the stochasticity of the simulations. Results for models 1 and 2 are presented in Figs. 11 and 12, respectively. More detailed statistics were obtained by performing larger-scale shear calculations for model 1 on a tissue of size $50 \times 50 = 2500$ cells, with 20 replicates. In this case, the calculations

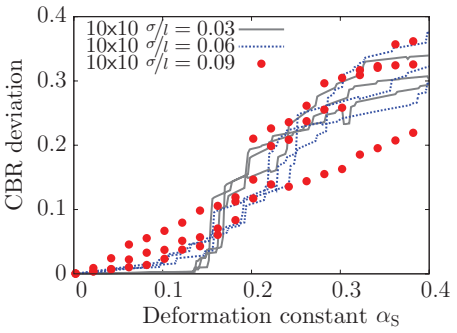

(a) Shear

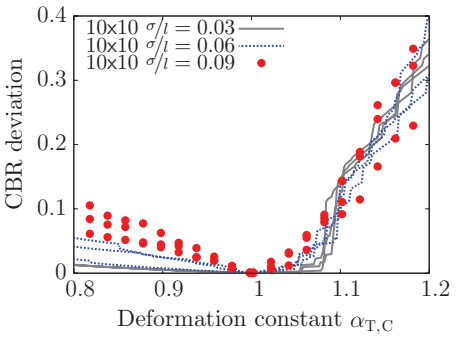

(b) Tension and compression

FIG. 11. (Color online) Series of plots showing how model 1 (center based and tessellation based) deviates from the CBR as the deformation parameter α varies for (a) shear and (b) tension and compression. Three values of the standard deviation ($\frac{\sigma}{\ell} = 0.03, 0.06,$ and 0.09) were used for the non-Brownian case and one size of tissue (10×10 cells). For each value of standard deviation, three replicates are plotted. Results were obtained by computing Eq. (8) in the central region for displacements prescribed on the boundary nodes using Eqs. (5)–(7). These plots show that (i) the CBR may not be valid when the reference configuration is an irregular lattice and (ii) for the lowest value of the standard deviation $\frac{\sigma}{\ell} = 0.03$, the CBR may still provide a good approximation to the displacement field.

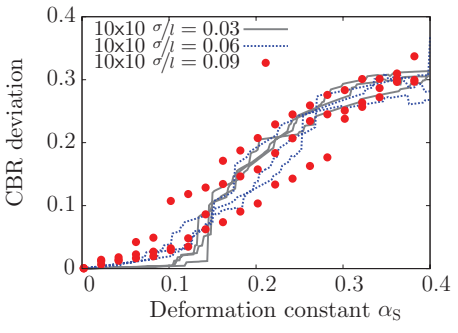

(a) Shear

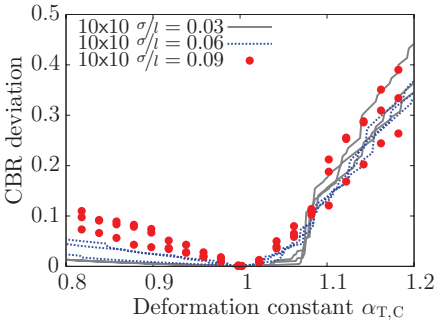

(b) Tension and compression

FIG. 12. (Color online) Series of plots showing how model 2 (center based and sphere based) deviates from the CBR as the deformation parameter α varies for (a) shear and (b) tension and compression. Three values of the standard deviation ($\frac{\sigma}{\ell} = 0.03, 0.06,$ and 0.09) were used for the non-Brownian case and one size of tissue (10×10 cells). For each value of standard deviation, three replicates are plotted. Results were obtained by computing Eq. (8) in the central region for displacements prescribed on the boundary nodes using Eqs. (5)–(7). These plots show that (i) the CBR is not valid when the reference configuration does not follow a regular lattice and (ii) for the lowest value of the standard deviation $\frac{\sigma}{\ell} = 0.03$, the CBR may still represent a good approximation of the displacement field.

were limited to small-amplitude deformations to avoid large computation times. Results are presented in Fig. 13 and an example simulation in Fig. 14. We remark that the qualitative behavior of the larger $50 \times 50 = 2500$ cells tissue and the $10 \times 10 = 100$ cells tissue are similar, but the amplitude of the deviations was significantly larger for the $50 \times 50 = 2500$ cells tissue. Although an interesting problem, it is beyond the scope of this paper to explore further the impact of the modes on the CBR deviation and the size dependence of the repartition of prestress in the initial relaxed configuration.

For both models and tissue sizes, our results show that the CBR is not exactly satisfied, even in the limit of small deformations. To understand why the CBR does not provide a good leading-order representation of the deformations, it is important to realize that the energy functional characterizing the mechanics of the cell population is sensitive to modifications in the standard deviation. In particular, although cells are initially in stable equilibrium, the number of nodes in the reference state that are close to bifurcation from local energy minima and the amount of prestress increase with σ. The system is, in some sense, in a metastable configuration.

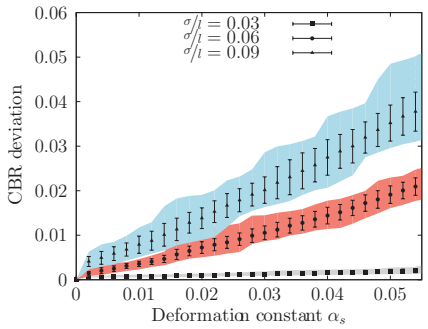

FIG. 13. (Color online) Series of plots showing how model 1 (center based and tessellation based) deviates from the CBR as the deformation parameter α varies for shear. Three values of the standard deviation ($\frac{\sigma}{\ell} = 0.03, 0.06,$ and 0.09) were used for the non-Brownian case and one size of tissue (50×50 cells). For each value of the standard deviation, 20 replicates were computed and the following statistics are presented: arithmetic mean (points), standard deviation (error bars), and min-max boundaries (uniformly shaded gray, red, and blue areas).

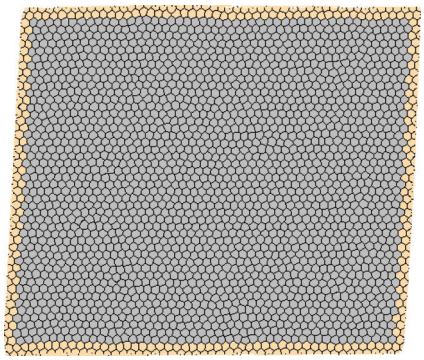

FIG. 14. (Color online) Voronoi tessellation corresponding to a shear deformation applied to a non-Brownian cell population (50×50) cells using model 1 with $\alpha_S = 0.058$ and $\frac{\sigma}{\ell} = 0.09$.

Under such conditions, even the slightest displacement of the boundary nodes may trigger rearrangement on cellular length scales (e.g., node permutations) and lead to failure of the CBR. These cellular-scale phenomena cannot be captured by solid-continuum models, even with higher-order or nonlocal theories. In this sense, the CBR provides a reliable measure of solidlike elastic behavior.

Such immediate changes in the topology upon application of strain or stress may be reduced by annealing (see [38]). This process consists of applying large-deformation tension-compression cycles to the initial relaxed state, so that the system is set into a lower-energy configuration and prestress is reduced. Further, disordered systems with no initial prestress may be obtained by modifying cell connectivities, as is done in [40]. It is unclear, however, whether prestress forms an integral part of biological tissue mechanics or should be neglected. This issue will not be addressed in the present work.

Conversely, we see that for relatively small values of the standard deviation, particularly when $\frac{\sigma}{\ell} = 0.03$, the CBR may provide an approximate representation of node displacements. We may thus extend the validity of the CBR, with a notion of quasivalidity in the limit of small deformations and low-level disorder. In such cases, elastic models derived using the CBR may adequately describe tissue mechanics. We remark that the concept of quasivalidity would be difficult to determine using an analytical approach and numerical simulations of cellular-scale models are, in this case, helpful in understanding model behavior.

B. Vertex-based model: Model 4

We now apply the same techniques to investigate the validity of the CBR for vertex-based tissue models. For model 4, the deviation (8) is plotted as a function of the deformation parameter α for shear in Fig. 15(a) and for compression and tension in Fig. 15(b). Results are presented for a tissue of size 10×10 both with (B) and without random motion (NB).

The results presented in Fig. 15 reveal that the behavior of the vertex-based model is markedly different from that of the other models. In particular, Fig. 15 shows that the CBR is never satisfied, even approximately. In the limit of small deformations, the average deviation increases linearly with the deformation constant, starting from zero in the reference configuration. This is evident both under shear [Fig. 15(a)]

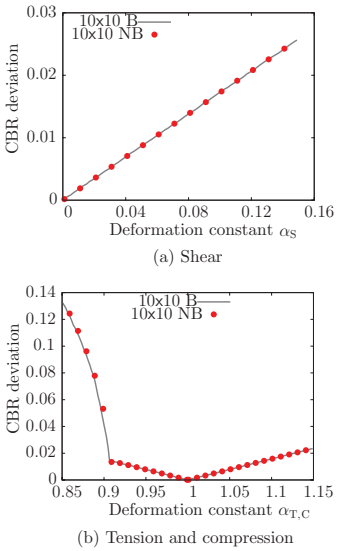

FIG. 15. (Color online) Plots of the deviation from the CBR for model 4 (vertex based and fixed connectivity) as a function of the deformation parameter α for (a) shear and (b) tension and compression experiments. For each plot, a tissue of size 10×10 cells was used for the Brownian and non-Brownian cases. Results were obtained by computing Eq. (8) in the central region for displacements prescribed on the boundary nodes using Eqs. (5)–(7). They show that (i) the CBR is not valid for vertex-based models even when the reference configuration follows a honeycomb lattice and (ii) there are two distinct regions, under compressive loading, of slow linear and fast nonlinear growth of the average deviation.

and under tension and compression [Fig. 15(b)]. The cause of this linear deviation is apparent from the spatial distribution of the nodes (see Fig. 16, where we have used $\alpha_S = 0.3$ to facilitate interpretation): The internal nodes slowly drift away from boundary nodes as they resist shape modification. To understand this phenomenon, recall that positions of vertices are determined by minimizing deformation (surface area of the cells) and interaction (boundaries of the cells) energies. While cell size in the internal region is constrained by the number of cells and the overall area of the region, cell edges or vertices are positioned via minimization of the interaction energy, a procedure that favors regular hexagons. Therefore, internal cells adopt a shape intermediate between that of the boundary cells and regular hexagons. This is also compatible with the idea that vertex-based models can be used for

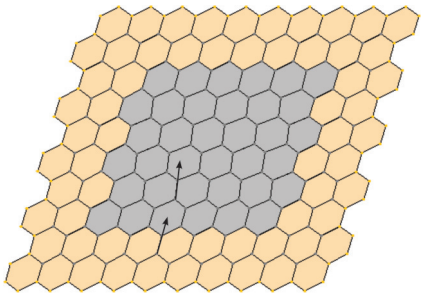

FIG. 16. (Color online) Linear drift corresponding to a shear deformation $\alpha_S = 0.3$ applied to a non-Brownian cell population (10×10 cells) described via model 4.

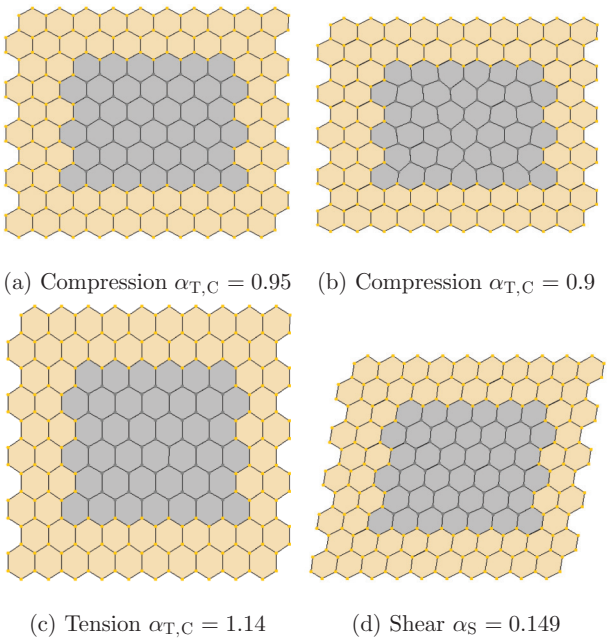

(a) Compression $\alpha_{\mathrm{T,C}} = 0.95$ (b) Compression $\alpha_{\mathrm{T,C}} = 0.9$

(c) Tension $\alpha_{\mathrm{T,C}} = 1.14$ (d) Shear $\alpha_{\mathrm{S}} = 0.149$

FIG. 17. (Color online) Sequence of events corresponding to shear and compression and tension deformations applied to a non-Brownian cell population (10×10 cells) described via model 4, with (a) compression $\alpha_{\mathrm{T,C}} = 0.95$, (b) tension $\alpha_{\mathrm{T,C}} = 1.14$, (c) compression $\alpha_{\mathrm{T,C}} = 0.9$, and (d) shear $\alpha_{\mathrm{S}} = 0.149$. These plots illustrate (i) the linear growth of the average deviation corresponding to a small drift of the central cells and (ii) the onset of instability corresponding to the nonlinear growth of the average deviation.

complex viscoelastoplastic rheology of foams (see, e.g., [41]). Interestingly, even though the CBR does not hold in this situation, the linearity of the deviation for small values of α and the spatial homogeneity of the cell behaviors suggest that a continuum model might still provide a good representation of the tissues mechanics as a whole. These results show that the CBR is not a necessary condition for continuumlike behavior, but rather acts as a measure of elastic, solidlike behavior.

We remark further that, under compressive loading, two different regimes can be identified. When the deformation constant is small, the deviation grows linearly with increasing α (see previous discussion) [Figs. 15(b) and 17(a)] until an instability occurs when $\alpha_{\mathrm{T,C}} \approx 0.9$ [see Fig. 17(b)]. This figure illustrates the inhomogeneous relaxation of vertex positions when α reaches the critical value of instability. We see that the deviation grows linearly with α until the shape incompatibility between internal and boundary nodes generates a reorganization of intermediate vertices. For larger values of α, the deviation is induced by an inhomogeneous drift and becomes nonlinear.

V. CONCLUSION AND DISCUSSION

In this paper, we have studied the validity of the CBR when applied to different cellular-scale models of biological tissues. We have found that the CBR holds for center-based models in the limit of small deformations. If the nodes in the reference configuration lie on a stress-free regular lattice, then we have shown that the CBR is exactly satisfied for the center-based models 1 (tessellation based with spring force), 2 (sphere based with quasispring force), and 3 (sphere based and nonlinear). If this is not the case, for example, if the rest lengths for intercellular forces are selected from a normal distribution, then the CBR can still provide a good approximation of node positions for low-disorder reference states and a domain of quasivalidity may be defined. If, however, the disorder is too large, most cells undergo inhomogeneous local rearrangements and a continuum solid description of the system is not possible. In this sense, the CBR provides a measure of continuum solidlike behavior.

In contrast, the vertex-based model is based on a different paradigm and does not satisfy the CBR, even for a lattice reference state in the limit of small deformations. In this case, cells are represented via vertices and cellular connectivity is fixed *ab initio*. For this model, we found that central cells deform more slowly than the boundary cells, leading to linear growth of the deviation from the CBR as α increases. We also remark that the homogeneous nature of the drift suggests that, even though the CBR fails, a continuum behavior may exist. This suggests that the CBR can be thought of as a measure of solidlike behavior, but may not be necessary for continuum behavior. Further, this suggests that the CBR will provide a good measure of continuumlike behavior in cases when deviation from the CBR is due to cellular-scale perturbations [i.e., Fig. 17(b)], but not when it is due to a homogeneous deviation of the whole tissue [i.e., Figs. 17(a), 17(c), and 17(d)].

These results open alternative perspectives in terms of hybrid and concurrent modeling of biological tissues. Indeed, approaches similar to that proposed in [11] imply that a clear connection exists between the discrete and continuum frameworks. As discussed in the Introduction, this connection is typically investigated in one dimension and seldom in two or three dimensions. Herein we have shown that in some situations, this connection can be made via the CBR. This bridge can be used to create a clear and explicit connection between continuum and discrete models, for instance, using a discrete virial expression of the stress tensor. Following this idea, hybrid blending over a boundary region could be used in a biological context. For instance, one could develop adaptive models that automatically switch between discrete and continuum descriptions on the basis of limit strain or stress criteria. Further, other atom-to-continuum methods could be adapted to tissue mechanics, such as adaptive quasicontinuum, bridge scale, or peridynamic methods. When compared with hybrid models, an advantage of such one-domain formulations is that cumbersome boundary conditions are not needed. The drawback, however, is that discretization of nonlocal formulations typically gives rise to dense matrices that are more difficult to invert than the sparse matrices produced by discretizing local models.

We have also demonstrated that the tissue-scale behavior of cellular-scale models involves a complex, nonlinear interplay between the model type (center based and vertex based), the cell connectivity, the forces, the set of parameters chosen, and even the nature of the deformation. For instance, if the cutoff length between nodes is set to be equal to the rest length, then attractive forces are completely eliminated and the CBR fails to describe node positions in the tension

regime. Paradoxically, we have also shown that very different constitutive laws for forces may behave similarly when compared via domains of validity of the CBR. Because of this complexity and nonlinearity, reliable classifications of cellular-scale models do not yet exist and are generally difficult to establish. Such classifications are desirable because of the increasing number of cellular-scale models in the literature and the difficulty in predicting their behavior. Interestingly, Murray *et al.* [42] proposed the classification of 1D forces via their behavior in the continuum limit by comparing nonlinear diffusion coefficients for cell density. This approach provides remarkable insight into the dynamics of tissue mechanics, but it is unclear how to generalize these 1D results to higher-dimensional systems. Therefore, here we suggest that this classification could be obtained by studying numerically the behavior of representative portions of tissue undergoing mechanical loading. In particular, we propose that the CBR could be used as a mechanical classification method for cellular-scale models, i.e., to test if models exhibit a macroscale solidlike behavior. A simple example of one such classification could be (a) models that conform with the CBR in the small-deformation limit, (b) models that approximately conform with the CBR in the small-deformation limit, or (c) models that do not conform with the CBR at all. With this idea, the classification method is adaptive and context dependent. For instance, model 2 with a cutoff length equal to the rest length is a member of (c) for tension deformation, while being a member of class (a) or (b) under compressive leading.

Future work should focus on (i) comparison with experimental data on tissue deformation, (ii) developing theories that apply to nonaffine situations, (iii) developing a complete classification method for cellular-scale models mechanics, (iv) exploring the influence of the reference state upon the macroscale mechanical properties of the tissue in more details (in particular, the impact of prestress), (v) adapting the CBR to account for homogeneous cellular growth, (vi) implementing hybrid concurrent models of biological tissues, and (vii) adapting other ATC strategies to the biological context.

In conclusion, this work has attempted to develop accurate continuous representations of cellular-scale models of biological tissues in more than one spatial dimension. Moreover, this approximation has allowed the comparison of different cellular-scale models, suggesting categories for such models. We anticipate that this work will eventually allow larger biological systems to be simulated more realistically using hybrid, discrete-continuum models.

ACKNOWLEDGMENTS

This work was based on work supported by Award No. KUK-C1-013-04, made by King Abdullah University of Science and Technology (KAUST).

APPENDIX

In this Appendix, we detail the intercellular forces that are used throughout this paper, starting with the spring force. On node i, this force may be written as

$$\mathbf{f}_i^S = \sum_j \mathbf{f}_{ij}^S \equiv \begin{cases} \lambda \frac{\mathbf{r}_{ij}}{\|\mathbf{r}_{ij}\|} \delta \ell & \text{for} \quad \delta \leqslant \frac{\ell_c}{\ell} \\ \mathbf{0} & \text{for} \quad \frac{\ell_c}{\ell} < \delta, \end{cases} \tag{A1}$$

where $\sum_j$ is the sum over the neighboring nodes, $\ell_{ij} > 0$ is the rest length of the spring that connects nodes i and j, and ℓ is a characteristic length scale (which we set equal to 10 μm). Unless stated otherwise, we assume that $\ell_{ij} = \ell$ for any pair i, j. Further, δ is the nondimensionalized overlap parameter defined by

$$\delta = \frac{1}{\ell}(\|\mathbf{r}_{ij}\| - \ell_{ij}). \tag{A2}$$

We also use a quasispring force defined by

$$\mathbf{f}_i^{\mathrm{QS}} = \sum_j \mathbf{f}_{ij}^{\mathrm{QS}} \equiv \begin{cases} \lambda \frac{\mathbf{r}_{ij}}{\|\mathbf{r}_{ij}\|} \ell \ln(1+\delta) & \text{for} \quad \delta \leqslant 0 \\ \lambda \frac{\mathbf{r}_{ij}}{\|\mathbf{r}_{ij}\|} \delta \ell \exp(-k\delta) & \text{for} \quad 0 < \delta < \frac{\ell_c}{\ell} \\ \mathbf{0} & \text{for} \quad \frac{\ell_c}{\ell} < \delta. \end{cases} \tag{A3}$$

In Eqs. (A1) and (A3), λ is the stiffness parameter, k is an adjustable parameter (representing cell-cell attraction), and ℓ_c is the cutoff length. Here we set $k = 0.5$, $\lambda = 15.0$ nN μm^{-1}, and $\ell_c = 1.1\ell = 11$ μm and all distances are expressed in μm. We remark that in the limit $\delta \ll 1$, we have

$$\mathbf{f}_{ij}^{\mathrm{QS}} = \mathbf{f}_{ij}^S + O(\delta^2), \tag{A4}$$

which means that quasispring and spring forces are equivalent at leading order in the limit of small overlap. The quasispring force is used to avoid possible instabilities encountered when using sphere-based models (for details see [37]).

We also consider a more complex description of cell mechanics using the nonlinear force

$$\mathbf{f}_i^{\mathrm{NL}} = \sum_j \mathbf{f}_{ij}^{\mathrm{NL}} \equiv \begin{cases} \mathbf{F}_{ij}^A + \mathbf{F}_{ij}^E + \mathbf{F}_{ij}^C & \text{for} \quad \delta \leqslant \frac{\ell_c}{\ell} \\ \mathbf{0} & \text{for} \quad \frac{\ell_c}{\ell} < \delta. \end{cases} \tag{A5}$$

In this expression, $\mathbf{F}_{ij}^A$ is the force component describing adhesive interactions between cells, $\mathbf{F}_{ij}^E$ is a force associated with the elastic properties of the cells, and $\mathbf{F}_{ij}^C$ is associated with compressibility effects. These forces are all conservative, so they can be uniquely defined via energy functionals. In this paper, we employ the forces used in [43] and the reader is referred to this paper for further details.

For vertex-based models, we consider only one type of conservative force that combines surface and volume energies, as described by Nagai and Honda [7] and Honda *et al.* [39]. We refer to this force as the Nagai-Honda force. It is defined as

$$\mathbf{f}_i^{\mathrm{NH}} = \nabla_i U, \tag{A6}$$

with

$$U = \sum_{\langle ij \rangle} \sigma_{\alpha\beta} |\mathbf{r}_i - \mathbf{r}_j| + \sum_\alpha \kappa \left(S_\alpha - S_\alpha^0\right)^2, \tag{A7}$$

where i and j are vertices, α and β are cells, distances are expressed in μm, $\sigma_{\alpha\beta} = 10$ nN is the boundary energy per unit length between cells α and β, $\kappa = 100$ nN μm^{-1} is a deformation parameter, S_α is the surface area of cell α, and S_α^0 is the equilibrium value of the surface area of cell α. For a more detailed description of these forces, the reader is referred to Fig. 1 and Eq. (6) in [7].

[1] T. Alarcòn, H. Byrne, and P. Maini, Prog. Biophys. Mol. Biol. **85**, 451 (2004).

[2] J. M. Osborne, A. Walter, S. K. Kershaw, G. R. Mirams, A. G. Fletcher, P. Pathmanathan, D. Gavaghan, O. E. Jensen, P. K. Maini, and H. M. Byrne, Philos. Trans. R. Soc. London Ser. A **368**, 5013 (2010).

[3] J. Moreira and A. Deutsch, Adv. Complex Syst. **5**, 247 (2002).

[4] F. Graner and J. A. Glazier, Phys. Rev. Lett. **69**, 2013 (1992).

[5] D. Drasdo and S. Höhme, Phys. Biol. **2**, 133 (2005).

[6] F. Meineke, C. Potten, and L. Loeffler, Cell Prolif. **34**, 253 (2001).

[7] T. Nagai and H. Honda, Philos. Mag. B **81**, 699 (2001).

[8] T. Newman, Math. Biosci. Eng. **2**, 611 (2005).

[9] P. Cundall and O. Strack, Geotechnique **29**, 47 (1979).

[10] D. Ambrosi and S. Pezzuto, J. Elast. **107**, 199 (2012).

[11] Y. Kim, M. A. Stolarska, and H. G. Othmer, Math. Models Methods Appl. Sci. **17**, 1773 (2007).

[12] M. A. Stolarska, Y. Kim, and H. G. Othmer, Philos. Trans. R. Soc. London Ser. A **367**, 3525 (2009).

[13] V. Shenoy, R. Miller, E. Tadmor, D. Rodney, R. Phillips, and M. Ortiz, J. Mech. Phys. Solids **47**, 611 (1999).

[14] G. Wagner and W. Liu, J. Comput. Phys. **190**, 249 (2003).

[15] J. Fish, M. A. Nuggehally, M. S. Shephard, C. R. Picu, S. Badia, M. L. Parks, and M. Gunzburger, Comput. Methods Appl. Mech. Eng. **196**, 4548 (2007).

[16] P. Seleson, M. Parks, M. Gunzburger, and R. Lehoucq, Multiscale Model. Simul. **8**, 204 (2009).

[17] S. Badia, M. Parks, P. Bochev, M. Gunzburger, and R. Lehoucq, Multiscale Model. Simul. **7**, 381 (2008).

[18] R. Miller and E. Tadmor, J. Comput. Aid. Mater. Des. **9**, 203 (2003).

[19] P. J. Murray, C. M. Edwards, M. J. Tindall, and P. K. Maini, Phys. Rev. E **80**, 031912 (2009).

[20] M. Bodnar and J. Velasquez, J. Differ. Equations **222**, 341 (2006).

[21] J. A. Fozard, H. M. Byrne, O. E. Jensen, and J. R. King, Math. Med. Biol. **27**, 39 (2010).

[22] M. Sheinman, C. P. Broedersz, and F. C. MacKintosh, Phys. Rev. E **85**, 021801 (2012).

[23] A. Aghaei, M. Abdolhosseini Qomi, M. Kazemi, and A. Khoei, Int. J. Solids Struct. **46**, 1925 (2009).

[24] G. Friesecke and F. Theil, J. Nonlin. Sci. **12**, 445 (2002).

[25] I. Stakgold, Q. Appl. Math. **8**, 169 (1950).

[26] M. Born and K. Huang, *Dynamical Theory of Crystal Lattices* (Oxford University Press, Oxford, 1954).

[27] J. Ericksen, Math. Mech. Solids **13**, 199 (2008).

[28] M. Zhou, Proc. R. Soc. London Ser. A **459**, 2347 (2003).

[29] S. Alexander, Phys. Rep. **296**, 65 (1998).

[30] C. Goldenberg, A. Tanguy, and J.-L. Barrat, Europhys. Lett. **85**, 16003 (2007).

[31] L. Gibson, J. Biomech. **38**, 377 (2005).

[32] B. Gumbiner, Cell **84**, 345 (1996).

[33] C. P. Broedersz, M. Sheinman, and F. C. MacKintosh, Phys. Rev. Lett. **108**, 078102 (2012).

[34] M. Gardel, K. Kasza, C. Brangwynne, J. Liu, and D. Weitz, *Mechanical Response of Cytoskeletal Networks in Methods in Cell Biology* (Elsevier, Amsterdam, 2008).

[35] J. Pitt-Francis, P. Pathmanathan, M. Bernabeu, R. Bordas, J. Cooper, A. Fletcher, G. Mirams, P. Murray, J. Osborne, A. Walter, S. Chapman, A. Garny, I. van Leeuwen, P. Maini, B. Rodriguez, S. Waters, J. Whiteley, H. Byrne, and D. Gavaghan, Comput. Phys. Commun. **180**, 2452 (2009); see also http://www.cs.ox.ac.uk/chaste/

[36] G. R. Mirams, C. J. Arthurs, M. O. Bernabeu, R. Bordas, J. Cooper, A. Corrias, Y. Davit, S.-J. Dunn, A. G. Fletcher, D. G. Harvey, M. E. Marsh, J. M. Osborne, P. Pathmanathan, J. Pitt-Francis, J. Southern, N. Zemzemi, and D. J. Gavaghan, PLoS Comput. Biol. **9**, e1002970 (2013).

[37] P. Pathmanathan, J. Cooper, A. Fletcher, G. Mirams, P. Murray, J. Osborne, J. Pitt-Francis, A. Walter, and S. J. Chapman, Phys. Biol. **6**, 036001 (2009).

[38] A. M. Kraynik, D. A. Reinelt, and F. van Swol, Phys. Rev. E **67**, 031403 (2003).

[39] H. Honda, M. Tanemura, and T. Nagai, J. Theor. Biol. **226**, 439 (2004).

[40] C. P. Broedersz, X. Mao, T. C. Lubensky, and F. C. MacKintosh, Nat. Phys. **7**, 983 (2011).

[41] C. Raufaste, B. Dollet, S. Cox, Y. Jiang, and F. Graner, Eur. Phys. J. E **23**, 217 (2007).

[42] P. J. Murray, C. M. Edwards, M. J. Tindall, and P. K. Maini, Phys. Rev. E **85**, 021921 (2012).

[43] P. Buske, J. Galle, N. Barker, G. Aust, H. Clevers, and M. Loeffler, PLoS Comput. Biol. **7**, e1001045 (2011).